Received: 18 March 2021 | Revised: 7 August 2021 | Accepted: 11 August 2021

DOI: 10.1002/fuce.202100037

Fuel Cells
From Fundamentals to Systems

ORIGINAL RESEARCH PAPER

Fuel flexibility of solid oxide fuel cells

Andre Weber

Institute for Applied Materials (IAM-ET), Karlsruhe Institute of Technology (KIT), Adenauerring 20b, Karlsruhe, Deutschland 76131, Germany

Correspondence
A. Weber, Institute for Applied Materials (IAM-ET), Karlsruhe Institute of Technology (KIT), Adenauerring 20b, D-76131 Karlsruhe, Germany.
Email: andre.weber@kit.edu

Funding information
Bundesministerium für Wirtschaft und Technologie, Grant/Award Numbers: 0327823B, 03ET2027B, 03ET6056E

Abstract

One of the major advantages of SOFCs is their high fuel flexibility. Next to natural gas and hydrogen, which are today's most common fuels for SOFC-systems and cell-/stack-testing respectively, various other fuels are applicable as well. In the literature, a number of promising results show that available fuels as propane, butane, ammonia, gasoline, diesel etc. can be applied. Here, the performance of an anode supported cell operated in specialized single cell test benches with different gaseous and liquid fuels and reformates thereof is presented. Fuels as ammonia, dissolved urea (AddBlue^{TM}), methane/steam and ethanol/water mixtures can directly be fed to the cell, whereas propane and diesel require external reforming. It is shown that in case of a stable fuel supply the cell performance with such fuels is similar to that of appropriate mixtures of H_2, N_2, CO, CO_2, and steam, if the impact of endothermic reforming or decomposition reactions is considered. Even though a stable fuel cell operation with such fuels is possible in a single cell test bench, it should be pointed out that an appropriate fuel processing will be mandatory on the system level.

KEYWORDS
AdBlue, ammonia, diesel, fuel flexibility, internal reforming, methane, propane, reformate, solid oxide fuel cell

INTRODUCTION

Research on fuel flexibility

Fuel flexibility is claimed to be a major advantage of solid oxide fuel cells. Already in early papers and reports the high fuel flexibility of fuel cells was highlighted [1,2]. A number of fundamental studies on hydrogen and hydrocarbon conversion in solid oxide cells exhibiting mostly noble metal (Pt, Au) electrodes dates back to 1960th and 1970th [3,4]. In the 1980th fuel flexibility with respect to various compounds such as CH_4, CH_2OH, CH_3OH, and C_2H_5OH was investigated still applying noble metal electrodes [5,6]. Later on the research was shifted toward technically relevant Ni-based cermet electrodes [7–10].

The direct electrooxidation of hydrocarbons in fuel cells is a holy grail since decades. In technical electrodes, typically exhibiting a thickness much larger than the electrochemically active part close to the electrolyte [11,12], a preferential contact of the fuel with a just catalytically active surface can hardly be avoided. Thus most likely reaction products of catalytically decomposed hydrocarbons as hydrogen will be the electrooxidized species, whereas the hydrocarbon itself is previously converted in an upstream catalytic reaction. The same holds for reformates and internally reformed hydrocarbons, only hydrogen will be

electrooxidized whereas other reformate species as CO will be catalytically converted [13]. In [14] performance and stability of an electrolyte supported cell with a Ni/YSZ cermet anode were evaluated, applying dry H_2, CO, CH_4, and mixtures thereof as the fuel. Unexpectedly, a stable operation of a conventional Ni/YSZ cermet anode in dry methane over a period of 1000 h was observed. Aging could be suppressed as the electrochemically generated steam and CO_2 avoided a severe coking, nevertheless a few mmš of the anode close to the gas inlet were affected after 1000 h.

As cracking of hydrocarbons and subsequent coking can hardly be avoided in the presence of a nickel catalyst, conventional Solid Oxide Fuel Cells (SOFCs) will hardly survive operation with dry hydrocarbons for thousands of hours. There have been a number of suggestions to prevent related aging mechanisms and failures such as infiltrating an appropriate catalyst into a Ni/YSZ anode [15], applying other metals instead of Ni [16,17], or adding a small amount of steam to the fuel [9]. Already in the 1980th, Steele [18] discussed the capability of oxide anodes to electrooxidize hydrocarbons and provided suggestions for the material design [19]. Experimental results on the fuel flexibility of such materials are presented in [20–24]. Considering such approaches mostly no long-term durability studies as well as no transfer into a stack were performed, only a few studies proved the technical feasibility of such concepts on the stack and system level [25].

Next to gaseous hydrocarbons the applicability of different (evaporated) liquid fuels was investigated in a number of studies. A stable power generation over several hours with decane, toluene, diesel, and other hydrocarbons was proven by Gorte [26–28] for Cu-based cermet anodes. Kishimoto showed a carbon deposition free operation with internally reformed $C_{12}H_{26}$ as a model fuel for kerosene using a Ni/ScSZ anode [10]. Liu [29] analyzed the performance and stability of a SDC-electrolyte-based cell with a number of hydrocarbon fuels of which only methanol provided a stable operation over 60 h whereas methane and ethanol led to a rapid degradation. To improve the anode with respect to (dry) ethanol electrooxidation different approaches are discussed in [30–32]. Kikuchi [33] showed that methane internal reforming proceeded without deterioration, whereas ethane and ethylene resulted in carbon deposition even at high steam-to-carbon ratios. In [34] it was shown that even small amounts (<0.5 vol.%) of C_2H_x hydrocarbons, which are typical residues in diesel reformates, lead to coking and a subsequent disintegration of the Ni/YSZ anode [35].

Ammonia — as a carbon free energy carrier — is another promising fuel for SOFC-applications. The capability of solid electrolyte cells to convert ammonia was already shown in 1980 [36]. Since that time a growing interest in NH_3 fed SOFCs is observed [37–41]. Cell and electrode development for ammonia conversion is reported including proton conducting cells [42–44]. Only a few papers deal with other N_xH_y-based fuels with ammonia forming compounds as a fuel. In [45], SOFC operation with hydrazine fuel was demonstrated. It was shown that catalytically decomposed N_2H_4 enabled a quite similar performance as an appropriate N_2/H_2 mixture. A thermodynamic analysis of urea as a fuel is discussed in [46], where electrochemical tests of a four cell stack showed that a fuel gas mixture of H_2, CO, N_2, H_2O, and CO_2 corresponding to "steam reformed" urea enables a performance quite similar to hydrogen fuel. To our best knowledge tests with urea or AdBlue™ have not been published so far even though its applicability is mentioned in [47].

Selection of fuels for fuel cells

With regard to a market introduction of fuel cells, the availability of a suitable fuel is an essential prerequisite. Especially during the initial phase, as well as for niche applications, the establishment of a refueling infrastructure is challenging. Thus fuels cells that are able to convert widely available fuels are given a significant advantage. Table 1 provides an overview of fuels that are already applied or considered for application in fuel cells. It should be noted that the given energy densities do not consider the tank or any additionally required BoP components for fuel processing. The fuel consumption was calculated based on the current equivalent of the fuel assuming a stack that is operating at 0.7 V cell voltage and 80% fuel utilization.

The applicability of a fuel will strongly depend on the application and size of the fuel cell system. Whereas for automotive applications compressed hydrogen is envisaged as the standard fuel for Polymer Electrolyte Membrane (PEM) fuel cell vehicles and a considerable number of refueling stations were put into operation in recent years, stationary systems (PEM and SOFC) operating on natural gas and (to a smaller extend) LPG are commercially available and about 360k systems are already installed in Japan, thereof about 10% operating on LPG [48].

Considering small mobile units, hydrogen, (direct [49]) methanol, or LPG [50] are the fuels of choice for low and high temperature fuel cells. Other fuels such as diesel, ethanol, ammonia or AdBlue™ have been evaluated in a number of cell/stack or system level tests but so far only limited fuel cell systems designed for such fuels are available.

The comparison of the fuels in Table 1 reveals that there is no "ideal" fuel that fulfills all requirements for any application. Hydrogen can be used in almost all kinds of fuel cells but a widespread stationary hydrogen supply is missing, limiting its applicability in stationary and

TABLE 1 Fuels for fuel cells, fuels already applied in fuel cell systems, or discussed for such application are compared with respect to their energy density, the resulting fuel consumption to provide 1 kW_{el} power (stack operating at 0.7 V cell voltage and 80% fuel utilization) and further considerable properties for their application in fuel cells. The fuel storage will be either in the **g**aseous or **l**iquid state, the related pressure values are given in brackets. With respect to fuel processing a more or less complex reforming (ref.) or evaporation (ev.) is required for most fuels

Fuel	Chemical composition of main components	Energy density (LHV) kWh kg^{-1}/kWh $L^{-1}_{(liquid)}$/kWh $m^{-3}_{(ideal\ gas)}$	Fuel consumption @ 1 kW_{el} g h^{-1}	Availability	Toxicity	Storage $g/l_{(p/bar)}$	Fuel processing	Sulfur removal	Applications
Hydrogen	H_2	33.4/2.4/3.0	67			$g_{(700)}$	—		
Natural gas	CH_4 (75-98%)	13.9/5.8/10.0	134			$g_{(200)}$	ref.		
Diesel	$C_{\sim 13}H_{\sim 24}$	11.5/10.4/92.7	158			l	ref.		
LPG	$\mathbf{C_3H_8}$ / C_4H_{10}	12.9/7.5/25.4	147			$l_{(<10)}$	ref.		
Ethanol	C_2H_6O	7.5/5.9/15.3	256			l	ref.		
Methanol	CH_3OH	5.5/4.4/7.9	356			l	ref.		
Ammonia	NH_3	5.2/3.5/4.0	378			$l_{(8.6)}$			
AdBlue™	$CH_4N_2O+H_2O$	0.95/1.04/0.99	2052			l	ev.		

industrial applications today. The same holds for small mobile systems. Actually hydrogen is not available "around the corner" and thus LPG (camping gas), ethanol, or AdBlue™ might be a better solution due to their 24/7 availability. Methanol and ammonia would be preferable considering a simple fuel processing, but might be unsuitable fuels for a daily use by the end customer due to their high toxicity and thus should be restricted to industrial fuel cell applications [51,52]. Diesel as well as gasoline attained large interest with respect to automotive applications and auxiliary power units [53,54] but the rather complex fuel processing including high temperature sulfur removal is challenging.

In this contribution, cell performance and stability are evaluated for a number of available fuels in single cell tests. All tests are performed with state-of-the-art anode supported cells. Fuels such as hydrogen (as a reference), methane, propane, diesel, an ethanol–water mixture, ammonia, and AdBlue™ are either directly supplied to the cell or a reformate composition, as analyzed at the outlet of an appropriate reformer, is supplied.

EXPERIMENTAL

Investigated cells

All electrochemical tests were performed on anode supported cells exhibiting a Ni/8YSZ anode substrate, a Ni/8YSZ anode functional layer, an 8YSZ electrolyte, a GDC diffusion barrier layer, and a LSCF cathode. The cells were manufactured at Research Center Jülich and/or CeramTec GmbH. In some cases, the GDC diffusion barrier layer and the LSCF cathode were screen printed and sintered at IAM-ET. Despite the different cell manufacturers the initial cell performance of all cells was quite similar (see Testing Procedures). Details regarding the manufacturing of these cells can be found in [55]. Microstructural features of anode substrate and functional layer are described in [56], impedance-based electrochemical models were presented in [57,58]. Further details of the electrochemical processes at the anode were analyzed for hydrogen [11,12] and reformate fuels [13]. In previous studies, the durability of these cells was investigated for nominal operation [59–61], sulfur poisoning [62,63], and coking conditions [34].

Single cell test bench

For most of the electrochemical tests in this study test benches for single cells exhibiting 1 cm^2 active electrode area were applied. Figure 1 displays the gas lines and the cell housing mounted inside a furnace. Details on this experimental setup and the common testing procedures are given in [64]. To supply liquid fuels as ethanol or AdBlue™ a modification of the test bench was necessary. An Al_2O_3 capillary was mounted into the Al_2O_3 fuel supply tube in the furnace. To provide a sufficient heat for evaporation, the capillary was heated by a Pt heating wire. The liquid fuels (AdBlue™, ethanol/water mixture) were provided by a Bronkhorst™ Liquiflow controller.

Testing procedures

The cells were started according to an internally developed heat up, anode reduction and formation procedure,

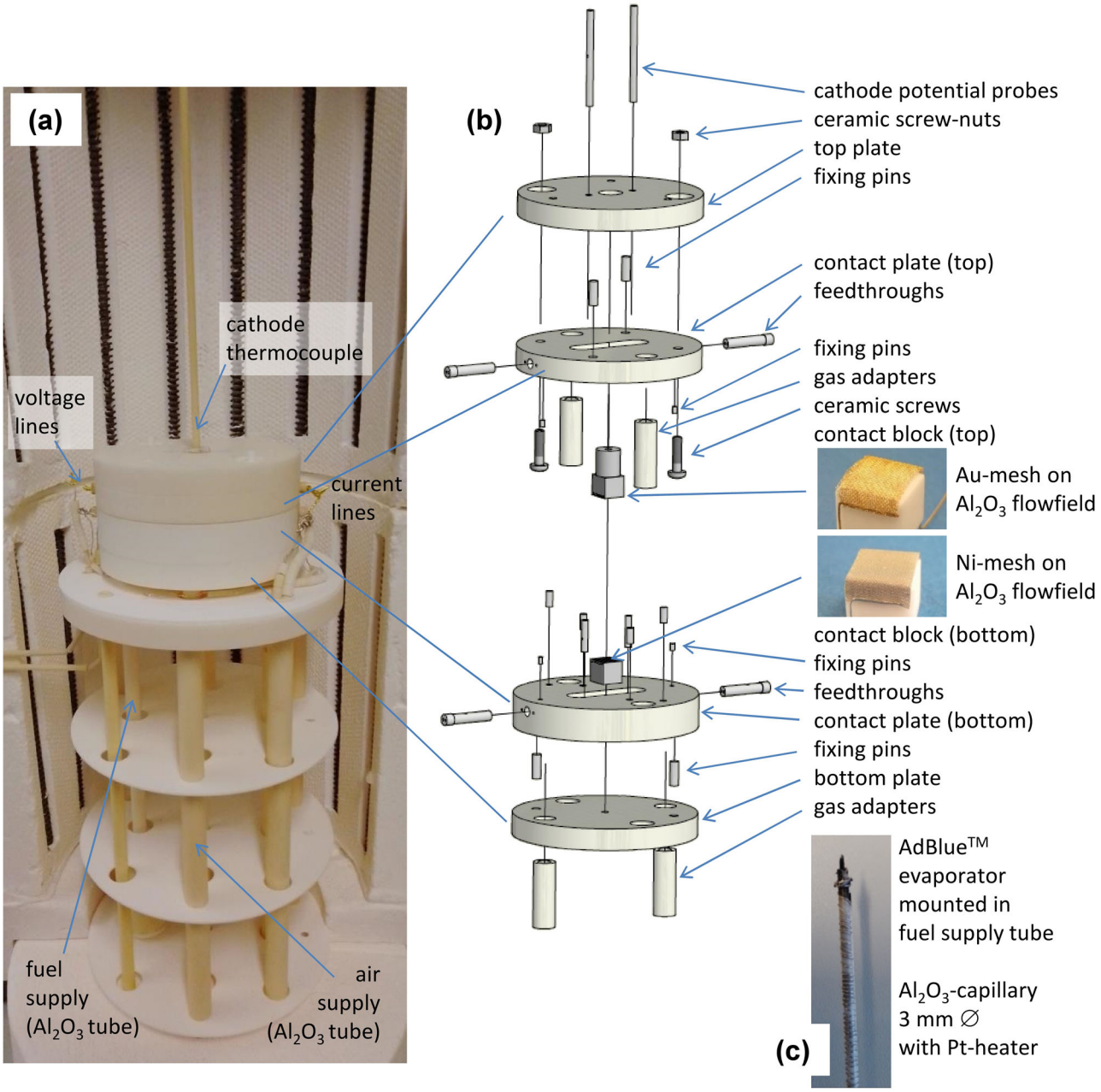

FIGURE 1 Gas supply and housing in the furnace of the (a) test bench, (b) Autocad™ 3D sketch of the ceramic (Al_2O_3) housing, and (c) evaporator used for the evaporation of AdBlue™ and the ethanol/water mixture

resulting in rather similar initial performance values (current density at 0.8 V cell voltage: 1.678 ± 0.124 A cm^{-2} at 801.5°C ± 1.14 K in air (250 sccm) / humidified hydrogen (250 sccm)). Only the cell tested in propane reformate was started up according to a different procedure. Here the NiO/YSZ anode was reduced in reformate fuel instead of hydrogen–nitrogen mixtures, which did not affect the later on evaluated cell performance in hydrogen.

A number of tests were performed including IV curves and impedance spectra at different operating conditions. The applied fuel compositions are listed in Table 2.

Hydrogen, ammonia, as well as the different reformates were provided via a gas mixing unit using gases from gas bottles (gas purity levels: O_2: 3.5, CO_2: 4.5, N_2: 5.0, H_2: 3.0, CO: 2.5, CH_4: 3.5, NH_3: 3.8). For internal reforming experiments the required amount of steam was generated in a burner unit and subsequently mixed to the methane fuel at a temperature of 180°C. In case of reformates and internal reforming a mixture of hydrogen, carbon monoxide, carbon dioxide, steam, and nitrogen was used. The steam was prepared in an upstream burner unit [64] and subsequently mixed to the fuel at a temperature of ~150°C. The

TABLE 2 fuel compositions applied in the single cell tests (composition in mol%, unless otherwise specified)

	H_2O	CO_2	N_2	H_2	CO	CH_4	NH_3	C_2H_6O	CH_4N_2O	H_2S/ppm
Hydrogen				100						
Int. ref. natural gas	66.67					33.33				
ext. ref. natural gas	15.23	4.76		64.78	15.23					
Sim. ref. (C-free)	20.00			80.00						
Diesel reformate	9.12	10.18	55.10	11.43	14.10	0.07				
Diesel reformate + H_2S	9.12	10.18	55.10	11.43	14.10	0.07				0.1
Propane reformate	1.00	1.00	47.00	28.00	22.00	1.00				
Ethanol + water	82.93							17.07		
Ammonia							100			
Decomposed ammonia			25.00	75.00						
AdBlue™	87.38								12.62	

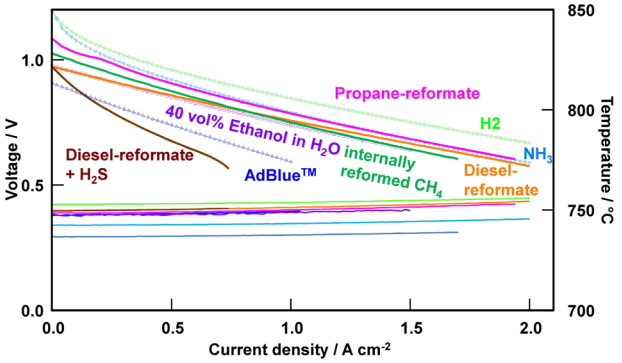

FIGURE 2 IV curves of the cells tested with the different fuel compositions listed in Table 2. The evaluated performance parameters are summarized in Table 3

residual amount of methane in reformates was considered by increasing the hydrogen and carbon monoxide amounts appropriately. Only in the durability test (Figure 8) various hydrocarbon mixtures were added to the base reformate. H_2S was supplied via an external gas supply unit (to avoid contamination of the gas supply system in the test bench). To enable the small amounts of H_2S, a bottled gas mixture containing 0.1 vol.% of H_2S in N_2 was used. The AdBlue™ applied in this study was bought at a petrol station nearby (Aral AdBlue™ according to ISO 22241); the ethanol/water mixture was prepared by mixing 40 vol.% ethanol and 60 vol.% deionized water. Compressed air was used as the oxidant in all tests.

To evaluate the impact of internal fuel processing including thermal effects, for some of the fuels (methane, ammonia) appropriate fuel mixtures, as expected after a complete conversion of the supplied fuel, were used as well. Impedance spectra were evaluated by the distribution of relaxation times (DRT). A more detailed analysis by CNLS fitting was not performed in this study.

RESULTS AND DISCUSSION

Cell performance

In Figure 2 IV curves of the cells tested with the different fuels are displayed. The cells were able to operate with all fuels but remarkable differences in cell performance with a factor of up to 3 are visible.

There are also differences in the shape of the IV curves. In case of dry fuels (H_2 and NH_3) the "activation polarization" behavior at low current densities has to be related to the fuel conversion [65] and the related decrease in electromotive force. In case of the propane reformate with just 1 vol.% of steam and CO_2 a quite similar behavior is observed, whereas in case of fuels exhibiting high portions

TABLE 3 Characteristic values of IV curves measured for the different fuel compositions according to Table 2

	OCV_{th} (V)	OCV_{IV} (V)	$I_{equivalent}$ (A)	$I_{(0.7\,V)}$ (A)	f.u. (%)	$T_{cell,OCV}$ (°C)	$T_{furnace}$ (°C)
Hydrogen	(–)	1.193	36	1.805	5.0	752.9	742.0
Int. ref. natural gas	1.019	1.023	36	1.216	3.4	736.4	768.0*
Ext. ref. natural gas	1.019	1.013	36	1.662	4.6	750.0	768.0*
Sim. ref. (C-free)	1.019	1.017	35	1.692	4.8	749.7	768.0*
Diesel reformate	0.977	0.973	17	1.307	7.9	749.8	742.0
Diesel reformate + H_2S	0.977	0.971	17	0.441	2.7	749.5	742.0
Propane reformate	1.084	1.085	15	1.418	9.2	748.5	742.0
Ethanol + water	0.990	0.976	14	1.194	8.8	748.5	742.0
Ammonia	(–)	1.197	36	1.436	4.0	742.4	742.0
Decomposed ammonia	(–)	1.200	36	1.451	4.0	751.9	742.0
AdBlue™	0.922	0.905	14	0.627	4.4	747.6	742.0

*Different furnace type, corresponding to T_{cell} value of 751.1°C for hydrogen operation.

of steam and CO_2 the IV curves are rather linear. There is a further difference in the sulfur-poisoned state (IV curve measured after 100 h of operation in H_2S-containing diesel reformate). In case of the H_2S-containing fuel, an additional overvoltage, which is attributed to an increased Butler–Volmer type activation polarization at the sulfur-poisoned Ni electrocatalyst in the anode, is observed.

Table 3 provides more details on these results. In column 2 and 3 the theoretical open circuit voltage OCV_{th} and the measured value from the IV curve (OCV_{IV}) are compared. OCV_{th} is calculated by means of the Nernst equation using the oxygen partial pressures in the oxidant (air, $pO_{2,ox} = 0.21$ atm) and the fuel ($pO_{2,fuel}$). The latter was calculated based on the fuel composition (Table 2) using the Gibbs Energy Minimizer in the thermodynamic software package MALT [66]. The targeted operating temperature of 750°C was considered in these calculations. As $pO_{2,fuel} = 0$ atm for (pure) hydrogen and ammonia, the theoretical open circuit voltage should be infinite ($OCV_{th} \rightarrow \infty$). For such fuels the measured open circuit voltage of the IV curve OCV_{IV} is determined by impurities in the fuel and the leakages in the cell, sealing and test bench. In case of AdBlue™ and ethanol the measured OCV is ~15 mV below the theoretical value, which might be related to deviations from the nominal fuel composition due to deviations in the supplied fuel mixture (31.8 to 33.2 wt.% urea according to DIN 70070) and an incomplete decomposition. For reformate fuels and internal reforming a good agreement with deviations ≤7 mV is observed.

The tests were performed in a test bench for the detailed electrochemical characterization of "incremental" cells, aiming at homogeneous operating conditions without lateral gradients in fuel composition or temperature over the entire active cell area (1 cmš). Thus all cells were operated with a high fuel excess. The current equivalent of the supplied fuels $I_{equivalent}$ is ranging between 14 and 35 A, resulting in fuel utilization values below 10%. Considering the cell temperature T_{cell}, measured by a thermocouple <2 mm above the cathode surface, some differences are observable despite the identical furnace temperature $T_{furnace}$. The lowest cell temperatures observed for internally reformed methane and ammonia can be related to the endothermal steam reforming of CH_4 (206 kJ mol^{-1}) and decomposition of NH_3 (46 kJ mol^{-1}), respectively. In case of AdBlue™ and ethanol/water the evaporation and subsequent decomposition reactions occur at much lower temperatures and will most probably take part in the upstream gas line close to the heated evaporator. In case of the reformates the supplied gas compositions are already close to equilibrium at 750°C and only negligible amounts of the constituents will be converted by the exothermic water gas shift reaction (−41 kJ mol^{-1}).

Impedance spectroscopy and DRT analysis

The evaluation of the fuel's impact on the polarization behavior and cell performance by means of impedance spectroscopy is challenging. In Figure 3 impedance spectra for the different fuels (a) and the related DRTs (b) are displayed. All spectra were measured under OCV conditions. Rather large polarization resistance values are obtained for ammonia and hydrogen as well as sulfur-containing diesel reformate. To visualize all DRTs in one plot a logarithmic scale of the *Y*-axis was chosen.

According to these spectra, fuels such as dry hydrogen and NH_3 should lead to the lowest cell performance, which is contradictory to the cell performance evaluated by means of the current density at a cell voltage of 0.7 V (Table 3). The reason for this behavior is the gas conversion and diffusion polarization [65,67] that is significantly enhanced if dry fuels are applied and impedance

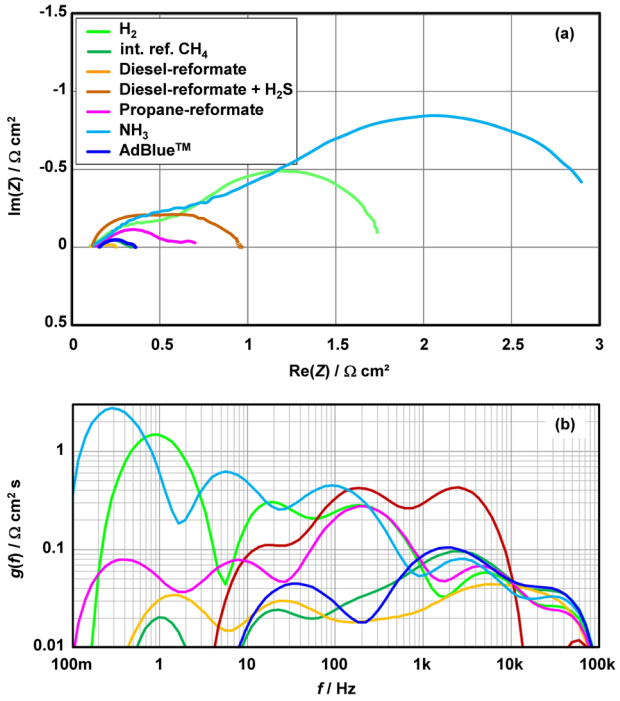

FIGURE 3 Impedance spectra (a) and the related DRTs (b) for the different fuel compositions. All spectra were measured under OCV conditions at temperatures as given in Table 3

spectra are measured at OCV conditions. This impact of fuel humidification is visualized in Figure 4. An increase in the steam content corresponding to a fuel utilization of 60% (Figure 4b) results in a drastic decrease in polarization resistance (>factor 10). The comparison between hydrogen, a H_2/N_2 mixture corresponding to decomposed ammonia (dec. NH_3) and ammonia fuel reveals differences in the low frequency peak (peak frequencies: 0.3 to 1 Hz) of the DRT (Figure 4c). These differences are mainly related to the fuel dilution by nitrogen whereas the NH_3 decomposition shows only a minor impact on the low frequency peak (peak frequencies of 0.5 Hz for decomposed ammonia and 0.3 Hz for ammonia fuel). The comparison of decomposed ammonia and ammonia fuel in a humidified state (Figure 4d) reveals much smaller differences in the polarization behavior. The increase in the ohmic resistance ASR_Ω (high frequency intercept at 1 MHz) has to be attributed to the temperature difference induced by the endothermal ammonia decomposition. Such effects related to endothermal catalytic processes will be discussed in the next section.

The spectra at high humidity are more meaningful concerning a rating of the cell performance obtainable with different fuels. In Figure 5 DRTs of those spectra are displayed. The differences between hydrogen and ammonia fuel are significantly smaller and the different electrochemical processes according to [57] are detectable in both cases. For internally reformed methane and diesel reformate the additional low frequency peak at 1–2 Hz related to carbon monoxide conversion via the watergas shift reaction [13] becomes visible. This process is suppressed by sulfur poisoning as visible in Figure 3, furthermore the sulfur poisoning leads to a shift of the anode processes toward lower relaxation frequencies [62] resulting in an overlap with the cathode process P_{2C} at ~100 Hz (Figure 5). In case of AdBlue™ operation, significant changes as a much

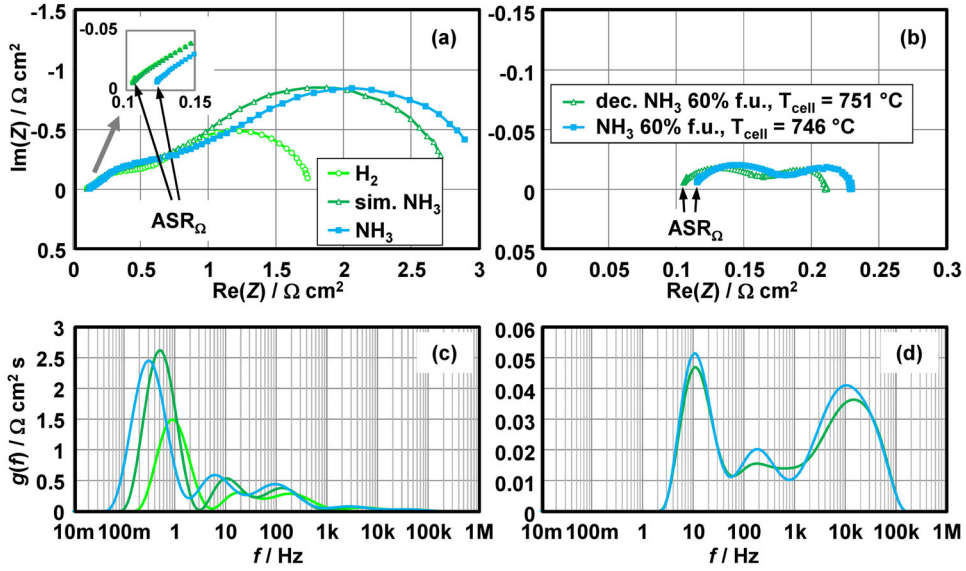

FIGURE 4 (a,b) Impedance spectra and (c,d) the related DRTs for hydrogen, ammonia, and a simulated ammonia fuel (corresponding mixture of H_2 and N_2) for (a,c) the dry fuels and (b,d) a simulated fuel utilization of 60% (60% of the supplied fuel replaced by appropriate amounts of steam and N_2)

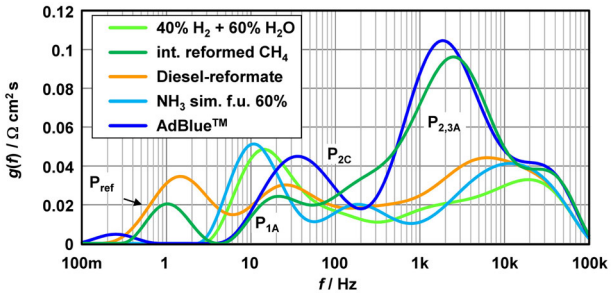

FIGURE 5 Comparison of DRTs — humidified hydrogen, internally reformed methane, diesel reformate, ammonia (with a simulated fuel utilization of 60%) and AdBlue™

larger contribution around 2 kHz (anode electrochemistry) and a shift of the gas diffusion process to higher frequencies are observable, which have not been further investigated in this study.

Impact of endothermal catalytic reactions

Figure 6a displays the temperature dependency of ASR_Ω for two cells. The first was tested in H_2, decomposed NH_3, and NH_3. Whereas the measured values are on one straight line for hydrogen and decomposed ammonia (appropriate mixture of $H_2 + N_2$), in case of ammonia fuel a shift toward higher values is observed. This has to be related to a local cooling of the cell by the endothermal ammonia decomposition. The cell temperature T_{cell} measured close to the cathode surface is lower for ammonia fuel. As the ASR_Ω is directly correlated with the internal cell temperature, for example, the temperature of the electrolyte [68], we have to conclude that the temperature of the cell's electrolyte is even below the measured cell temperature. In Figure 6b, the OCV values for hydrogen, decomposed ammonia, and ammonia are shown in a temperature range from 600 to 800°C. In the whole temperature range the measured values for H_2 and decomposed NH_3 are close to the theoretical OCV considering 0.48% H_2O (H_2) and 0.3% H_2O (NH_3) in the fuel. These small amounts of H_2O are typical leakage values observed for anode supported cells in this type of test bench. In case of NH_3, a decrease in OCV is observable for temperatures below 700°C, which is attributed to an incomplete decomposition of the supplied NH_3 at decreased operating temperatures.

The second cell displayed in Figure 6a was tested with (i) internally reformed methane (int. ref.), (ii) a fuel composition corresponding to external reformed methane (ext. ref., equilibrium composition at 750°C), and (iii) an appropriate mixture of hydrogen and steam (sim. ref.). Whereas for the latter two conditions a cell temperature T_{cell} of 750°C is achieved at a furnace temperature $T_{furnace}$ of 768°C, in case of internal reforming the cell temperature is decreased by 14 K. Increasing the furnace temperature to 781°C results in a T_{cell} value of 750°C. Despite the similar cell temperature, the ASR_Ω is still above the expected value (ΔASR_Ω = 20 mΩ cm^2). A further increase of the furnace temperature — considering the thermal activation of the ohmic resistance of the cell — to 800°C leads to the desired ASR_Ω. Thus it can be concluded that endothermic internal reforming results in a significant decrease (~33 K) of the electrolyte temperature even in a small size single cell.

The quantitative analysis reveals a clear relation between the cooling power provided by endothermal reactions and the decrease in cell temperature. In case of steam reforming ~8.8 W (0.0625 nlmCH_4, S/C = 2, assuming a complete catalytic conversion to equilibrium composition according to Table 2) is provided. This heat consumption at the cell decreased the measured cell temperature from 750.0°C (cell supplied with an equilibrated reformate mixture) to 736.4°C (cell supplied with an appropriate methane/steam mixture). In case of ammonia a cooling power of ~5.7 W that is related to the endothermal decomposition of ammonia (0.167 nlm NH_3) has to be expected, which resulted in a cell temperature decrease from 751.9°C (cell supplied with a H_2/N_2 mixture according to decomposed NH_3) to 742.4°C for operation with ammonia fuel. The observed cooling of 1.55 K/W (steam reforming) and 1.67 K/W (ammonia decomposition) are both in a similar range. It should be noted that these values will strongly depend on cell size, housing, and test bench.

In Figure 7a related IV curves for the abovementioned testing conditions are displayed. It is obvious that the increase of the furnace temperature to 800°C results in a similar cell performance for internal reforming as achieved with external reforming/a simulated (carbon free) reformate fuel. This result shows that the apparently lower cell performance for internal reforming of methane (~26% decrease in power density) is solely related to the reduced temperature inside the cell. Furthermore there is no performance difference between correspondingly humidified hydrogen, the reformate composition containing appropriate amounts of CO and CO_2 and internally reformed methane. This is to be expected considering that only hydrogen is electrooxidized in the anode, whereas carbon monoxide is converted by the watergas shift reaction and methane is already reformed in the outer part of the anode substrate.

The DRTs displayed in Figure 7b show a corresponding result. There are no significant differences with respect to the anode processes $P_{2,3A}$ as long as an appropriate furnace temperature compensating the cooling effect of the endothermal reforming reaction is selected. In case of lower temperatures the thermally activated processes $P_{2,3A}$

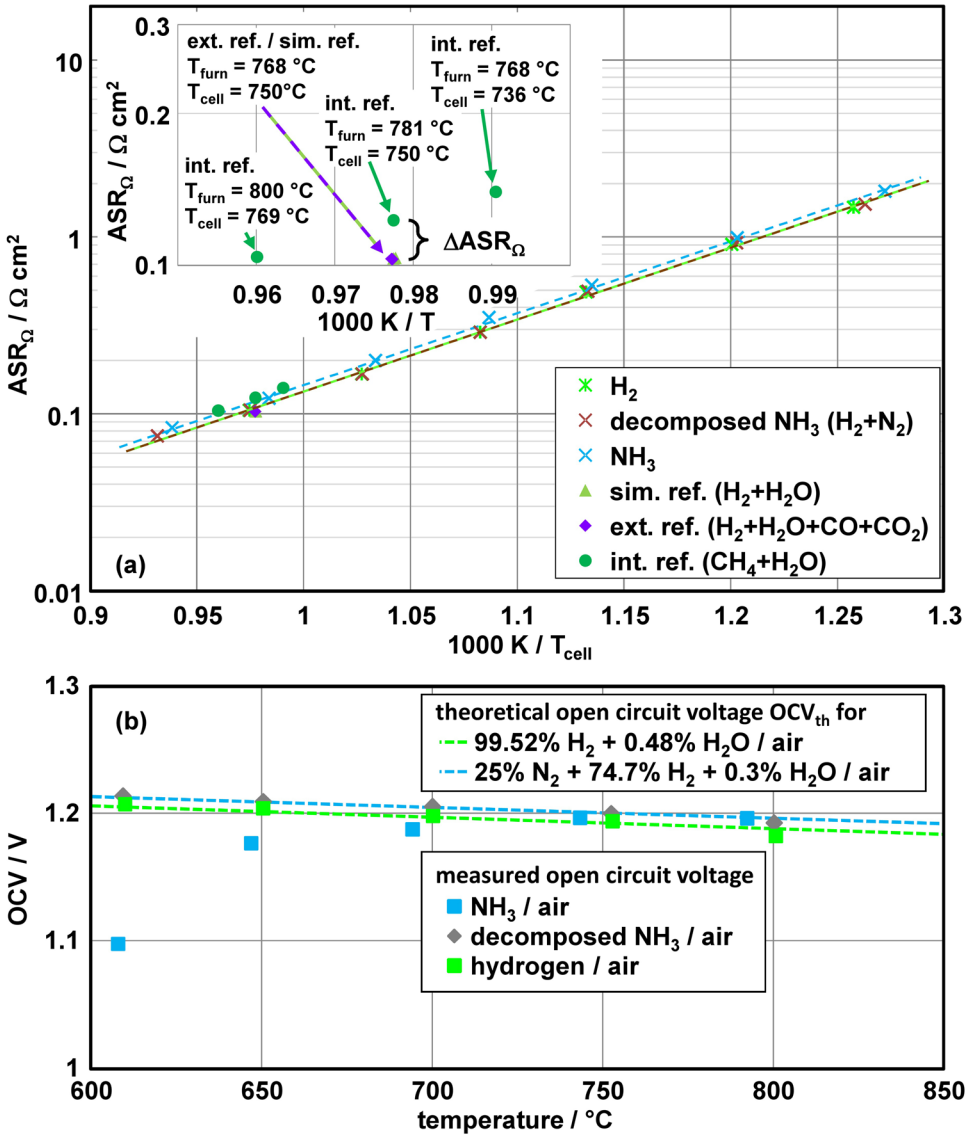

FIGURE 6 Temperature dependency of the ohmic resistance. (a) Comparison of hydrogen/a H_2/N_2 mixture corresponding to decomposed ammonia/ammonia and simulated CH_4 reformate (carbon free) / a fuel composition corresponding to external reformed CH_4 / internal reformed CH_4. (b) The OCV values for hydrogen/a H_2/N_2 mixture corresponding to decomposed ammonia and ammonia

(hydrogen electrooxidation in the cermet anode [11,12]) and P_{2C} (cathode electrochemistry [69]) are increased. The process P_{1A} representing the H_2/H_2O gas diffusion in the anode substrate is larger for hydrogen operation whereas the additional low frequency process P_{ref} at ~1 Hz [13,70] solely occurs for the CO/CO_2-containing fuels.

Stability and durability

Concerning durability, the steady state operation with stable reformate compositions did not cause any severe problem and degradation rates quite similar to humidified hydrogen were observed. This can be related to the fact that the electrochemical reaction is limited to hydrogen and the conversion of carbon monoxide occurs via the watergas shift reaction [13]. In case of an improper reforming, resulting in residual higher hydrocarbons (C_mH_n with $m \geq 2$), or impurities as sulfur-compounds, a rapid degradation within hours was observed [34,35,63]. Cycling, which will be unavoidable in applications as APU, can become crucial and regeneration strategies [47] will be required. Especially during system and reformer start-up it will be critical to avoid higher hydrocarbons, which might result in carbon deposition and subsequent metal dusting of the anode if a propane or diesel reformate is used. Thus next to mechanical stress arising from thermal cycling the anode can be affected by the fuel gas.

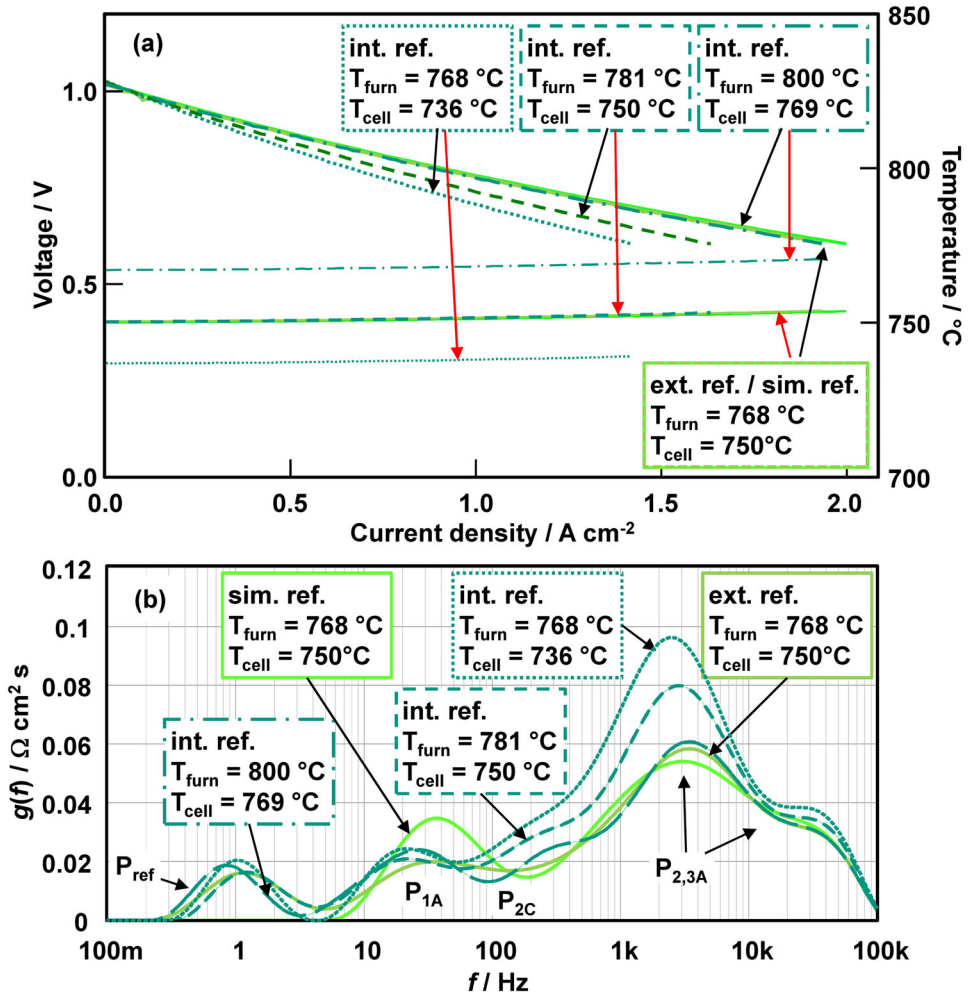

FIGURE 7 (a) I/V characteristics and (b) DRT for simulated CH_4 reformate (carbon free) / a gas mixture corresponding to external reformed CH_4 / internal reformed CH_4

To evaluate the stability, testing in reformate mixtures corresponding to the reformer outlet gas composition is required. In a single cell test shown in Figure 8, the impact of various hydrocarbon compounds in diesel reformate is evaluated. In this test different reformate compositions including small amounts of higher hydrocarbons measured beforehand at the outlet of an optimized diesel reformer were fed to the cell. Despite this, the cell showed an excellent stability over an operating time of ~3000 h.

Durability tests with higher hydrocarbons are challenging because next to the cell itself, the test bench might be affected. The break for the modification of the test bench (Figure 8, 800 to 1900 h) was required because of carbon deposition and clogging of the Al_2O_3 gas lines. By a modification of the gas supply system this problem could be eliminated.

It should be noted that in single cell tests even with dry hydrocarbons or alcohols a stable cell performance can be achieved as long as these compounds are already cracked in the gas lines and only the gaseous products, mainly hydrogen, are fed to the cell. In this case, after some hours to weeks of continuous testing, a clogging of the gas supply will take place. In the 1 cmš single cell tests performed in this study, such an effect was only observed for the ethanol–water mixture. After about 20 h of continuous operation the fuel flow rate decreased due to a clogging of the evaporator, which was originally designed for the evaporation of AdBlue™.

In Figure 9 a short-term stability test with evaporated AdBlue™ as the fuel is displayed. A stable operation is at least possible for several 100 h (the test was stopped intentional at t = 360 h). During this test even an increase in cell voltage can be observed. Impedance spectra and the DRT-based impedance analysis revealed a decrease of the ohmic resistance as well as some changes in the polarization behavior. With respect to AdBlue™ a more detailed analysis of the electrochemistry and a correlation with the different ammonia decomposition products is required.

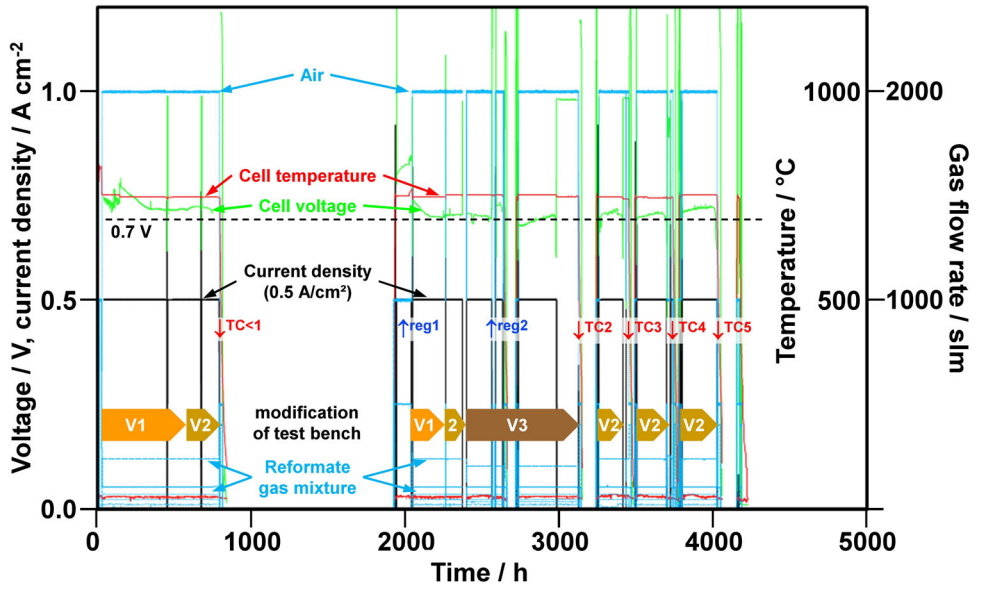

FIGURE 8 3000 h durability test with simulated diesel reformate. In this test carried out on a 16 cm^2 ASC a reformate composition different from the one in Table 1 was applied, namely 14.32% H_2, 14.93% CO, 52.59% N_2, 8.44% H_2O, 9.21% CO_2, and 0.43% hydrocarbons. Three hydrocarbon mixtures were applied (V1–V3) exhibiting 100% methane (V1), 65.39% methane + 0.84% C_2H_2 + 19.77% C_2H_4 + 6.52% C_2H_6 + 7.49% C_3H_6 (V2), and 64.27% methane + 0.82% C_2H_2 + 19.43% C_2H_4 + 6.41% C_2H_6 + 7.36% C_3H_6 + 1.71% benzene (V3). A cell voltage around 0.7 V was achieved at a current density of 500 mA cm^{-2} and a fuel utilization of 75%

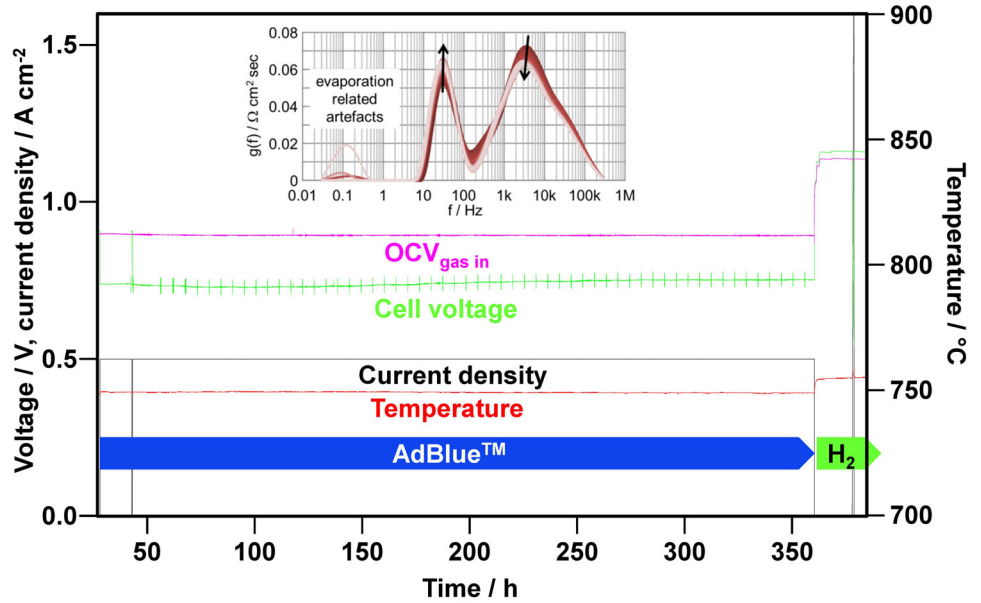

FIGURE 9 Short-term stability test using commercial AdBlue™ as the fuel. The increase in cell voltage is related to a decrease in ohmic resistance (35 mΩ cm^2) during the test, the changes of the polarization processes (see DRT inlay) resulted in an additional decrease of 4 mΩ cm^2

CONCLUSIONS

In this contribution the impact of different gaseous and liquid fuels on the performance and stability of anode supported cells was analyzed. Hydrogen, different types of methane, propane, and diesel reformate; ethanol; ammonia; and AdBlue™ were applied. The cells could be operated with all fuels investigated in this study. OCV values closed to the theoretical ones (deviation < 20 mV) were measured. Significant differences in cell performance were

observed, which have to be attributed to the compositions of the fuels respectively the evolving products. A comparison at a nominal operating temperature of 750°C revealed cell performances of 440 to 1800 mA cm^{-2} (current density at 0.7 V cell voltage) at operating temperatures between 732 and 754°C . The observed differences in cell temperature have to be attributed to the endothermal reforming and decomposition reactions of the fuel. Such thermal effects have to be considered in single cell tests as they can affect the cell performance seriously.

Based on these results a high fuel flexibility of a state-of-the-art SOFC can be confirmed. At least in single cell tests a direct supply of a variety of different fuels is feasible. Considering the observed impacts as cooling due to endothermal reactions or carbon deposition due to an incomplete catalytic conversion, in most cases an appropriate upstream fuel processing will remain mandatory for stacks and systems.

ACKNOWLEDGMENTS

Funding by the Bundesministerium für Wirtschaft und Technologie (BMWi 0327823B, 03ET2027B, and 03ET6056E) is gratefully acknowledged.

ORCID

Andre Weber https://orcid.org/0000-0003-1744-3732

REFERENCES

1. C. G. Peattie, *IEEE spectrum* **1966**, *3*, 69.
2. J. M. King Jr, *Advanced Technology Fuel Cell Program. Final Report, United Technologies Corp*, Power Systems Div, South Windsor, CT **1976**.
3. J. Weissbart, R. Ruka, *J. Electrochem. Soc.* **1962**, *109*, 723.
4. T. H. Etsell, S. N. Flengas, *J. Electrochem. Soc.* **1971**, *118*, 1890.
5. B. G. Ong, C. C. Chiang, D. M. Mason, *Solid State Ionics* **1981**, *3–4*, 447.
6. B. C. Nguyen, *J. Electrochem. Soc.* **1986**, *133*, 1807.
7. K. Eguchi, H. Kojo, T. Takeguchi, R. Kikuchi, K. Sasaki, *Solid State Ionics* **2002**, *152–153*, 411.
8. G. J. Saunders, K. Kendall, *J. Power Sources* **2002**, *106*, 258.
9. H. Sumi, K. Ukai, Y. Mizutani, H. Mori, C. J. Wen, H. Takahashi, O. Yamamoto, *Solid State Ionics* **2004**, *174*, 151.
10. H. Kishimoto, K. Yamaji, T. Horita, Y. Xiong, N. Sakai, M. E. Brito, H. Yokokawa, *J. Power Sources* **2007**, *172*, 67.
11. S. Dierickx, T. Mundloch, A. Weber, E. Ivers-Tiffée, *J. Power Sources* **2019**, *415*, 69.
12. S. Dierickx, J. Joos, A. Weber, E. Ivers-Tiffée, *Electrochim Acta* **2018**, *265*, 736.
13. A. Kromp, A. Leonide, A. Weber, E. Ivers-Tiffée, *J. Electrochem. Soc.* **2011**, *158*, B980.
14. A. Weber, B. Sauer, A. C. Müller, D. Herbstritt, E. Ivers-Tiffée, *Solid State Ionics* **2002**, *152*, 543.
15. J. M. Klein, M. Hénault, C. Roux, Y. Bultel, S. Georges, *J. Power Sources* **2009**, *193*, 331.
16. A. Cantos-Gomez, R. Ruiz-Bustos, J. Van Duijn, *Fuel Cells* **2011**, *11*, 140.
17. R. J. Gorte, H. Kim, J. M. Vohs, *J. Power Sources* **2002**, *106*, 10.
18. B. C. H. Steele, I. Kelly, H. Middleton, R. Rudkin, *Solid State Ionics* **1988**, *28–30*, 1547.
19. B. C. H. Steele, P. H. Middleton, R. A. Rudkin, *Solid State Ionics* **1989**, *40–41*, 388.
20. E. Lay, G. Gauthier, S. Ã. Rosini, C. Savaniu, J. T. S. Irvine, *Solid State Ionics* **2008**, *179*, 1562.
21. B. D. Madsen, S. A. Barnett, *Solid State Ionics* **2005**, *176*, 2545.
22. R. Kikuchi, N. Koashi, T. Matsui, K. Eguchi, T. Norby, *J. Alloys Compd.* **2006**, *408–412*, 622.
23. M. Lo Faro, V. Antonucci, P. L. Antonucci, A. S. Aricò, *Fuel* **2012**, *102*, 554.
24. K. J. Pan, A. M. Hussain, E. D. Wachsman, *J. Power Sources* **2017**, *347*, 277.
25. M. C. Verbraeken, B. Iwanschitz, E. Stefan, M. Cassidy, U. Weissen, A. Mai, J. T. S. Irvine, *Fuel Cells* **2015**, *15*, 682.
26. S. Park, J. M. Vohs, R. J. Gorte, *Nature* **2000**, *404*, 265.
27. G. M. Crosbie, E. P. Murray, D. R. Bauer, H. Kim, S. Park, J. Vohs, R. J. Gorte, *SAE Tech. Pap.* **2001**, *110*, 651.
28. H. Kim, S. Park, J. M. Vohs, R. J. Gorte, *J. Electrochem. Soc.* **2001**, *148*, A693.
29. M. Liu, R. Peng, D. Dong, J. Gao, X. Liu, G. Meng, *J. Power Sources* **2008**, *185*, 188.
30. B. Huang, X. J. Zhu, W. Q. Hu, Q. C. Yu, H. Y. Tu, *J. Power Sources* **2009**, *186*, 29.
31. H.x. You, G.d. Gao, L. Zhou, A. Abuliti, *J, Fuel Chem. Technol.* **2010**, *38*, 116.
32. M. Lo Faro, S. C. Zignani, A. S. Aricò, *J. Electrochem. Soc.* **2019**, *91*, 1845.
33. R. Kikuchi, K. Eguchi, *J. Japan Pet. Inst.* **2004**, *47*, 225.
34. H. Timmermann, W. Sawady, D. Campbell, A. Weber, R. Reimert, E. Ivers-Tiffée, *J. Electrochem. Soc.* **2008**, *155*, B356.
35. A. Weber, in *Encyclopedia of Electrochemical Power Sources* (Ed. J. Garche), Elsevier, Amsterdam **2009**, pp. 120.
36. R. D. Farr, C. G. Vayenas, *J. Electrochem. Soc.* **1980**, *127*, 1478.
37. A. Wojcik, H. Middleton, I. Damopoulos, J. van Herle, *J. Power Sources* **2003**, *118*, 342.
38. A. Fuerte, R. X. Valenzuela, M. J. Escudero, L. Daza, *J. Power Sources* **2009**, *192*, 170.
39. G. Cinti, G. Discepoli, E. Sisani, U. Desideri, *Int. J. Hydrogen Energy* **2016**, *41*, 13583.
40. A. F. S. Molouk, J. Yang, T. Okanishi, H. Muroyama, T. Matsui, K. Eguchi, *J. Power Sources* **2016**, *305*, 72.
41. A. Hagen, H. Langnickel, X. Sun, *Int. J. Hydrogen Energy* **2019**, *44*, 18382.
42. W. Akimoto, T. Fujimoto, M. Saito, M. Inaba, H. Yoshida, T. Inagaki, *Solid State Ionics* **2014**, *256*, 1.
43. Q. MA, R. Peng, Y. Lin, J. Gao, G. Meng, *J. Power Sources* **2006**, *161*, 95.
44. K. Miyazaki, T. Okanishi, H. Muroyama, T. Matsui, K. Eguchi, *J. Power Sources* **2017**, *365*, 148.
45. J. Song, R. Ran, Z. Shao, *Int. J. Hydrogen Energy* **2010**, *35*, 7919.
46. F. Abraham, I. Dincer, *J. Power Sources* **2015**, *299*, 544.
47. T. Kiefer, A. Weber, US Patent US 9,640,827 B2, **2017**.
48. number of μCHP fuel cell systems installed in Japan, https://www.ace.or.jp/web/works/works_0090.html, **2020**.
49. Efoy-Comfort, https://www.efoy-comfort.com/de, **2021**.
50. C. Geipel, K. Hauptmeier, K. Herbrig, F. Mittmann, M. Münch, M. Pötschke, L. Reichel, T. Strohbach, T. Seidel, A. Surrey, C. Walter, *J. Electrochem. Soc.* **2019**, *91*, 123.

51. J. Rechberger, R. Schauperl, J. B. Hansen, P. K. Larsen, *J. Electrochem. Soc.* **2019**, *25*, 1085.
52. J. B. Hansen, P. V. Hendriksen, *J. Electrochem. Soc.* **2019**, *91*, 2455.
53. J. Tachtler, T. Dietsch, G. Götz, *SAE Technical Paper Series* **2000**, *2000-01-0374*.
54. P. Lamp, J. Tachtler, O. Finkenwirth, P. Mukerjee, S. Shaffer, *Fuel Cells* **2003**, *3*, 146.
55. N. H. Menzler, F. Tietz, S. Uhlenbruck, H. P. Buchkremer, D. Stöver, *Journal of Materials Science* **2010**, *45*, 3109.
56. J. Joos, M. Ender, I. Rotscholl, N. Menzler, E. Ivers-Tiffée, *J. Power Sources* **2014**, *246*, 819.
57. A. Leonide, V. Sonn, A. Weber, E. Ivers-Tiffée, *J. Electrochem. Soc.* **2008**, *155*, B36.
58. A. Leonide, S. Hansmann, A. Weber, E. Ivers-Tiffée, *J. Power Sources* **2011**, *196*, 7343.
59. C. Endler-Schuck, A. Leonide, A. Weber, S. Uhlenbruck, F. Tietz, E. Ivers-Tiffée, *J. Power Sources* **2011**, *196*, 7257.
60. C. Endler-Schuck, J. Joos, C. Niedrig, A. Weber, E. Ivers-Tiffée, *Solid State Ionics* **2015**, *269*, 67.
61. C. Endler, A. Leonide, A. Weber, F. Tietz, E. Ivers-Tiffée, *J. Electrochem. Soc.* **2010**, *157*, B292.
62. A. Kromp, S. Dierickx, A. Leonide, A. Weber, E. Ivers-Tiffée, *J. Electrochem. Soc.* **2012**, *159*, B597.
63. A. Weber, S. Dierickx, A. Kromp, E. Ivers-Tiffée, *Fuel Cells* **2013**, *13*, 487.
64. D. Klotz, A. Weber, E. Ivers-Tiffée, *Electrochim. Acta* **2017**, *227*, 110.
65. S. Primdahl, M. Mogensen, *J. Electrochem. Soc.* **1998**, *145*, 2431.
66. H. Yokokawa, S. Yamauchi, T. Matsumoto, *Calphad* **2002**, *26*, 155.
67. S. Primdahl, M. Mogensen, *J. Electrochem. Soc.* **1999**, *146*, 2827.
68. D. Klotz, J. C. Njodzefon, A. Weber, E. Ivers-Tiffée, *ECS Trans.* **2012**, *45*, 523.
69. A. Leonide, B. Rüger, A. Weber, W. A. Meulenberg, E. Ivers-Tiffée, *ECS Trans.* **2009**, *25*, 2487.
70. A. Kromp, H. Geisler, A. Weber, E. Ivers-Tiffée, *Electrochim. Acta* **2013**, *106*, 418.

How to cite this article: A. Weber, *Fuel Cells* **2021**, 1. https://doi.org/10.1002/fuce.202100037